Optical Materials 46 (2015) 414–417

Contents lists available at ScienceDirect

Optical Materials

journal homepage: www.elsevier.com/locate/optmat

Passively Q-switched Nd:YVO_4 waveguide laser using graphene as a saturable absorber

Ruiyun He [a], Javier R. Vázquez de Aldana [b], Feng Chen [a,*]

[a] School of Physics, State Key Laboratory of Crystal Materials, Shandong University, Jinan 250100, China
[b] Laser Microprocessing Group, Universidad de Salamanca, Salamanca 37008, Spain

ARTICLE INFO

Article history:
Received 23 March 2015
Received in revised form 27 April 2015
Accepted 1 May 2015
Available online 13 May 2015

Keywords:
Optical waveguides
Q-switched waveguide lasers
Laser material processing
Graphene saturable absorber

ABSTRACT

We report on passively Q-switched lasers in femtosecond laser written waveguide in Nd:YVO_4 crystal. Using graphene as a saturable absorber, passively Q-switched waveguide laser operations are achieved along both TE and TM polarizations with single modal profiles. Furthermore, all-angle linear light pump was utilized to investigate the thorough information of the polarization effects of the laser, showing that the optimum polarization for laser generation is TE. The maximum average output power is estimated to be 129 mW with 12.2% slope efficiency, corresponding to single-pulse energy of 8.1 nJ, pulse duration of 25.0 ns and repetition rate of 16.3 MHz.

1. Introduction

Integrated photonic devices are based on the processing of light confined in compact optical structures called optical waveguides [1]. Among several techniques developed for waveguide fabrication, three-dimensional (3D) direct femtosecond laser writing has been regarded as an efficient and promising technique to fabricate diverse optical waveguides in various transparent optical materials [2–7], since the pioneering work of Davis et al. [8]. There are many unique advantages in favor of femtosecond laser writing of waveguides over other fabrication techniques including metal-ion indiffusion [9], ion/proton exchange [10], epitaxial layer deposition [11], and ion-beam implantation/irradiation [12]. Femtosecond laser writing appears as a direct, rapid, mask-free fabrication technique which can construct 3D waveguides with spatial resolution down to ~100 nm resolution. Femtosecond laser pulses with high intensities induce extremely localized alteration of the refractive index through nonlinear absorption processes. The refractive index modification of the femtosecond laser irradiated regions could be either positive or negative, due to the combined effect of material nature and laser parameters (repetition rate, wavelength, polarization, pulse energy, focusing conditions, scanning speed, etc.). In general, there are three main types of femtosecond laser writing waveguides depending on the waveguide core configuration [5–7]. Type I waveguides consist of a waveguide core with positive refractive index changes in the region directly irradiated by the femtosecond laser. It is quite easy and convenient for 3D fabrication of complex devices using the Type I configuration [13]. However, there are some disadvantages (e.g., bad thermo stability, hard to realize in crystals and only support guidance along one polarization) limiting the application of Type I waveguide [14]. Type II waveguides (also called stress-induced waveguides) locate in the region between parallel laser damage tracks with negative refractive index changes and possess a stress-optic refractive index increase in the center. So far, stable Type II waveguides have been achieved in several materials utilizing dual-line or multiple-line techniques [15–22]. Type III configuration (also called depressed cladding waveguides) consists of a core surrounded by a number of low-index femtosecond laser written tracks which are close one to each other. With well-preserved bulk features in the waveguide core, Type III waveguides could support guidance along both TE and TM polarizations [23–26].

Waveguide lasers with dimensions of micrometer have remarkable applications in integrated photonics, benefiting from the reduced lasing thresholds and comparable efficiencies with respect to bulk laser systems [27,28]. On the other hand, compact pulsed lasers are significant for a variety of applications including laser processing, optical imaging and optical fiber communication [2–7,29,30]. As one of the dominant techniques to generate pulsed lasers, passive Q-switching features a saturable absorber (SA) which has nonlinear optical absorption. Recently, graphene has emerged as an ideal SA benefiting from the low-cost, easy fabrication and the outstanding saturable absorption including the low

* Corresponding author. Tel.: +86 531 88363007; fax: +86 531 88363350.
E-mail address: drfchen@sdu.edu.cn (F. Chen).

http://dx.doi.org/10.1016/j.optmat.2015.05.001
0925-3467/

saturation intensity, high damage threshold, large modulation depth, ultrafast recovery time and ultra-broad absorption ranging from the visible to the THz waveband [31–33].

So far, optical waveguides have been realized in Nd:YVO_4 crystals fabricated by ion implantation/irradiation [34,35], thermal diffusion [36], pulsed laser deposition [37] and femtosecond laser writing (type II dual-line [17–19] and circular depressed cladding configurations [23,24]). Also reported are the continuous-wave (CW) laser operations. In this work, we report on the fabrication of Nd:YVO_4 Type II waveguides implemented by four femtosecond laser damage tracks, and the graphene-based Q-switched pulsed laser oscillation at 1064 nm in the Nd:YVO_4 waveguides.

2. Experimental methods

The *a*-cut Nd:YVO_4 crystal sample (doped by 2 at.% Nd^{3+} ions) was cut with sizes of $9(c) \times 7(b) \times 2(a)\,mm^3$ and optically polished. An amplified Ti:Sapphire femtosecond laser (Spitfire, Spectra Physics, USA), which produced pulses of 120 fs duration, 1 mJ maximum pulse energy at a repetition of 1 kHz and linearly polarized at 800 nm, was utilized to fabricate waveguides in Nd:YVO_4 crystal. The pulse energy was reduced to 2.1 μJ by employing a calibrated neutral density filter placed after a half-wave plate and a linear polarizer. The laser beam was focused at a depth of ~110 μm below the largest sample surface through a 40× microscope objective (N.A. = 0.65). The scanning velocity was set to be 50 μm/s. Under these conditions, severe damage tracks are produced by the laser and a significant amount of stress is induced in the neighborhood of the track. The line scan procedure was repeated four times at different depths (*a*-axis direction) and lateral positions (*c*-axis direction) of the sample by scanning the sample along the *b*-axis direction. The separation between the two sets of femtosecond laser written tracks was chosen to be 20 μm along the *c*-axis direction. Along the *a*-axis direction (depth), two femtosecond laser tracks were laid end to end.

The guiding performance was carried out by utilizing a typical end-face arrangement. Microscope object lens and convex lens were employed to couple the light into and out of the waveguides. In the passive operation regime, a linearly polarized CW solid state laser with wavelength of 1064 nm was employed to investigate the guiding properties of the waveguides. Based on the end-face arrangement, the Q-switched waveguide laser operation experiments were performed by end pumping, as illustrated in Fig. 1. A polarized light beam at a wavelength of 820 nm, generated from a tunable CW Ti:Sapphire laser (Coherent MBR PE) at room temperature, was used as the pump source. A half-wave plate (P) and a Glan-Taylor polarizer (G) were utilized to adjust the input power and polarization. The pump laser was coupled into the waveguide by a convex lens (L_1) with a focus length of 25 mm, which has a good match with the waveguide mode field diameter. The Fabry–Perot laser cavity was formed by the two polished end facets without additional dielectric mirrors. The inset in Fig. 1 shows the microscope image of the waveguide cross section taken by using a metalloscope (Axio Imager, Carl Zeiss) operating in transmission mode. For the Q-switched pulsed laser generation, a graphene film (~5 layers) coated quartz mirror was employed as the saturable absorber (GSA). The graphene film coated quartz plate was provided by XFNANO Materials Tech Co., Ltd, Nanjing, China. The graphene thin film was grown by chemical vapor deposition (CVD) on copper and nickel firstly, with 5 layers measured by the Raman spectroscopy. Then, the graphene was transferred to a transparent quartz plate with a thickness of ~2 mm. The transmission of the graphene film coated quartz plate was measured to be ~81% at the wavelength of ~1064 nm. Afterwards, the graphene coated plate was adhere close to the output surface of Nd:YVO_4 crystal. The obtained pulse laser was collected by a 20× microscope objective lens (L_2) and imaged by using an IR CCD camera. A spectrometer with resolution of 0.4 nm was utilized to analyze the emission spectra of the waveguide laser.

3. Results and discussion

The femtosecond laser induced negative refractive-index changes in the directly irradiated regions, causing expansion of the lattices in the focal volume. The waveguide core was therefore located in the region between the two sets of tracks and possessed a relatively high index through the stress-induced effects. Fig. 2 shows the near-field modal profiles of the Nd:YVO_4 multiple-line waveguide at 1064 nm along TE (i.e., polarization parallel to *c*-axis) and TM (i.e., polarization parallel to *a*-axis) polarizations, respectively. As one can see, the output modes exhibit relatively symmetrical single mode distributions along both TE and TM polarizations, which is different from the Type II waveguides in cubic crystals (e.g., Nd:GGG [20], Nd:YAG [21]) and Ti:sapphire [22] as they only support guidance parallel to the damage tracks. The propagation losses of the Nd:YVO_4 waveguide were estimated to be ~1.2 dB/cm and ~1.9 dB/cm for the TE and TM polarizations, respectively.

Fig. 3(a) depicts the laser emission spectrum from Nd:YVO_4 waveguide from Nd:YVO_4 waveguide in graphene-SA Q-switched pulse laser. The central wavelength is ~1064.4 nm with the full width at half maximum (FWHM) bandwidth of ~0.8 nm. Fig. 3(b) shows the distribution of the near-field modal profiles of the pulsed laser oscillation generated from the Nd:YVO_4 multiple-line waveguide along two orthogonal polarizations (i.e. polarization parallel to *c*-axis or *a*-axis), respectively.

Fig. 4(a) plots the average output powers of Nd:YVO_4 waveguide pulsed lasers as a function of launched pump power. As the

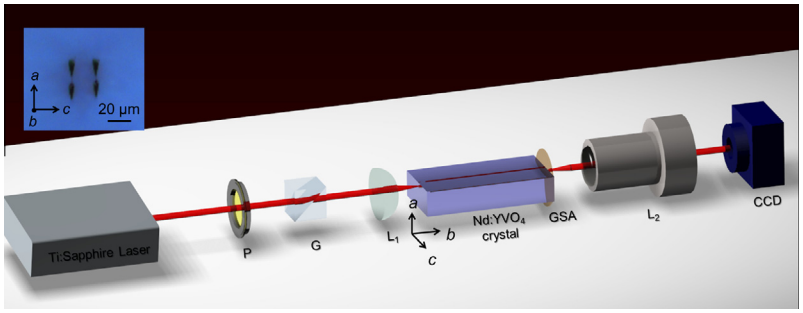

Fig. 1. Schematic plot of the experimental setup for graphene-based Q-switched waveguide laser operation. P: half-wave plate; G: Glan-Taylor polarizer; L_1: convex lens; GSA: graphene coated quartz mirror as the SA; L_2: microscope objective lens. The inset picture is the microphotograph of the cross section of Nd:YVO_4 waveguide consisting of four femtosecond laser writing tracks. The crystal axis of Nd:YVO_4 crystal are given.

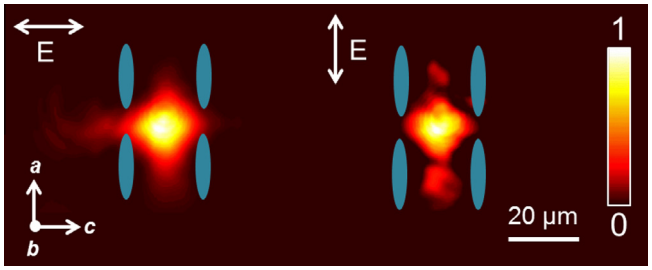

Fig. 2. Measured near-field modal profiles at 1064 nm of the femtosecond laser written Nd:YVO_4 waveguide. The crystal axis of Nd:YVO_4 crystal are given. The inserted arrows show the polarizations. Blue lines are added to indicate the locations of femtosecond laser writing tracks. (For interpretation of the references to color in this figure legend, the reader is referred to the web version of this article.)

launched pump power increases, the pulsed output laser powers climb to maximums at 129 mW and 83 mW with the highest available launched pump power of ~1.2 W and ~1.24 W for the TE and TM polarizations, corresponding to optical conversion efficiencies (i.e., rate of output to incident power) of 10.8% and 6.7%, respectively. From the linear fit of the experimental data, the lasing threshold (P_{th}) of the pulsed output laser are determined to be 114 mW and 197 mW for the TE and TM polarizations, respectively. Fig. 4(b) shows the dependence of average output power on all-angle linear polarization of the 950 mW pump laser. As one can see, the maximum output powers occur at $\theta = 0°$ (i.e., polarization parallel to *c*-axis) and the minimum appear at $\theta = 90°$ (i.e., polarization parallel to *a*-axis), which indicates the anisotropy effect induced by the femtosecond laser pulses in the Type II waveguide. In addition, post-annealing treatment could be utilized to further optimize the waveguide lasing performance by reducing the guiding attenuation introduced by femtosecond laser writing [38].

Investigations on the characteristics of the laser pulse show that the graphene-based Q-switched laser can reach the minimum pulse duration (25.0 ns/31.5 ns), the maximum repetition rate (16.3 MHz/13.8 MHz) and the maximum pulse energy (8.1 nJ/6.0 nJ) under the maximum pump power (1.2 W/1.24 W) along TE/TM polarization. Fig. 5 shows the dependence of the pulse duration, pulse energy and repetition rate as functions of the launched power collected from the Q-switched pulse waveguide laser along TE polarization. By varying the pump power, the repetition rate could be tuned from 3.8 MHz to 16.3 MHz. The approximate linear variation of repetition rate with increasing launched pumping power is a typical and reasonable phenomenon in passively Q-switched pulsed lasers. With the increasing the pump power from 0.13 W to 1.2 W, the pulse duration values present downtrend on the whole in spite of the existence of some fluctuations, varying from 115.0 ns to 25.0 ns. Meanwhile, the single pulse energy increases from ~1.6 nJ to ~8.1 nJ. The inset picture in Fig. 5 present the Q-switched pulse laser oscilloscope traces under the pumping power of ~1.05 W. In this case, the average output power

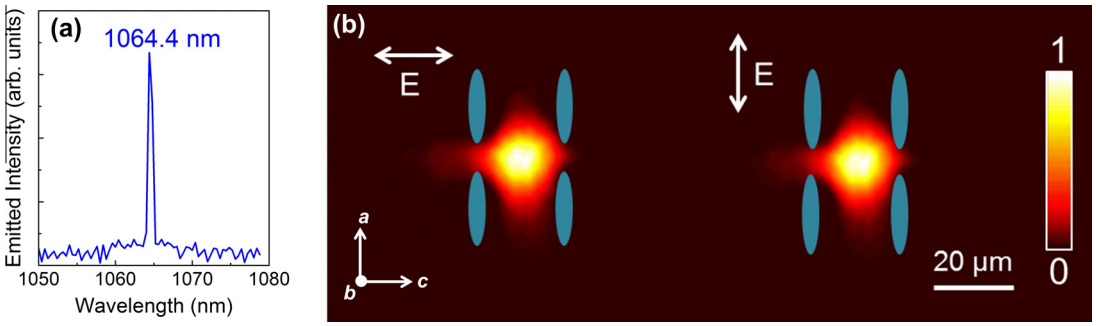

Fig. 3. (a) Laser emission spectrum from the femtosecond laser written Nd:YVO_4 waveguide. Peak position stays at 1064.4 nm and the FWHM is 0.8 nm. (b) Measured near-field modal profiles of the pulsed laser oscillation collected from the femtosecond laser written Nd:YVO_4 waveguide. The crystal axis of Nd:YVO_4 crystal are given. The inserted arrows show the polarizations. Blue lines are added to indicate the locations of femtosecond laser writing tracks. (For interpretation of the references to color in this figure legend, the reader is referred to the web version of this article.)

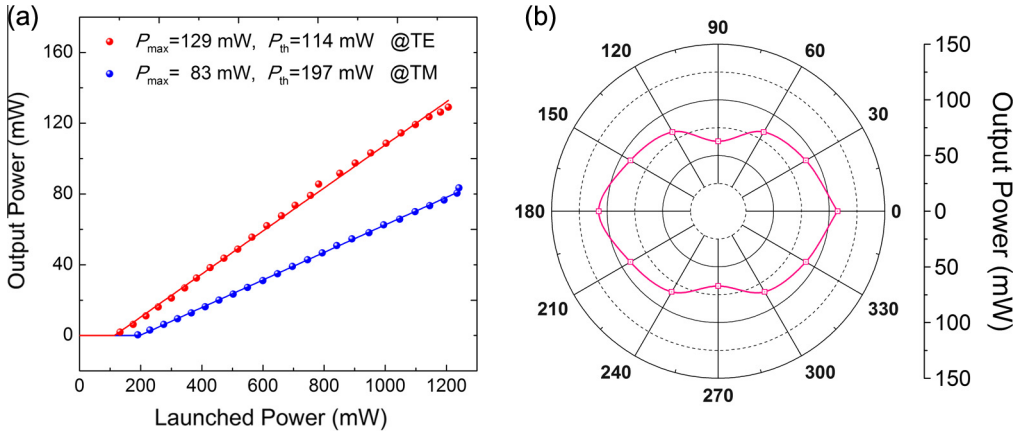

Fig. 4. (a) Average output power as a function of the launched power along TE (red) and TM (blue) polarizations, respectively. The solid lines represent the linear fit of the experimental data. (b) Polar image of the output power of the Q-switched pulsed laser pumped by all-angle linear polarized laser at the same launched power of 950 mW. (For interpretation of the references to color in this figure legend, the reader is referred to the web version of this article.)

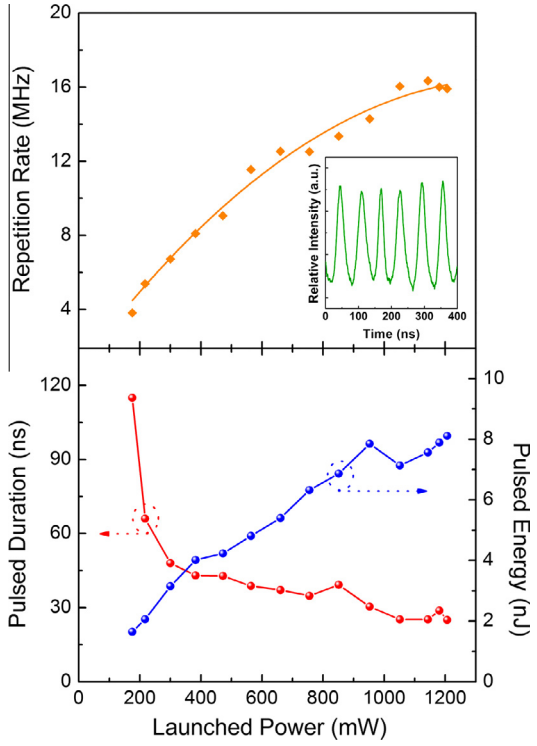

Fig. 5. Q-switched pulse duration (red), pulse energy (blue) and repetition rate (orange) versus launched pump power. The inset picture shows a typical pulse train (green). (For interpretation of the references to color in this figure legend, the reader is referred to the web version of this article.)

was 114 mW. The corresponding Q-switched single-pulse energy was 7.1 nJ with 25.2 ns pulse duration and 16.0 MHz pulse repetition.

4. Conclusion

We report on a passively Q-switched waveguide laser employing a graphene coated quartz plate as the SA. The 1064 nm pulsed laser was generated from a Type II multiple-line waveguide produced by direct femtosecond laser writing in Nd:YVO_4 crystal. The waveguide supports laser operation along both TE and TM polarizations with polarization effect. The maximum average output power was 129 mW obtained along the TE polarization, corresponding to a single-pulse energy of 8.1 nJ, pulse duration of 25.0 ns and repetition rate of 16.3 MHz.

Acknowledgments

This work was supported by the National Natural Science Foundation of China (No. 11274203) and Ministerio de Economía y Competitividad under Project FIS2013-44174-P, Spain.

References

[1] E.J. Murphy, Integrated Optical Circuits and Components: Design and Applications, Marcel Dekker, New York, 1999.
[2] R.R. Gattass, E. Mazur, Nat. Photon. 2 (4) (2008) 219–225.
[3] M. Ams, G.D. Marshall, P. Dekker, J. Piper, M.J. Withford, Laser Photon. Rev. 3 (6) (2009) 535–544.
[4] K. Sugioka, Y. Cheng, Light Sci. Appl. 3 (2014) e149.
[5] F. Chen, J.R. Vázquez de Aldana, Laser Photon. Rev. 8 (2) (2014) 251–275.
[6] D. Choudhury, J.R. Macdonald, A.K. Kar, Laser Photon. Rev. 8 (6) (2014) 827–846.
[7] T. Calmano, S. Müller, IEEE J. Sel. Top. Quant. Electron. 21 (1) (2015) 1602213.
[8] K.M. Davis, K. Miura, N. Sugimoto, K. Hirao, Opt. Lett. 21 (21) (1996) 1729–1731.
[9] D. Jaque, E. Cantelar, G. Lifante, Appl. Phys. B 88 (2) (2007) 201–204.
[10] A. Tervonen, B.R. West, S. Honkanen, Opt. Eng. 50 (7) (2011) 071107.
[11] R.W. Eason, T.C. May-Smith, C. Grivas, M.S.B. Darby, D.P. Shepherd, R. Gazia, Appl. Surf. Sci. 255 (10) (2009) 5199–5205.
[12] F. Chen, Laser Photon. Rev. 6 (5) (2012) 622–640.
[13] D.G. Lancaster, S. Gross, H. Ebendorff-Heidepriem, K. Kuan, T.M. Monro, M. Ams, A. Fuerbach, M.J. Withford, Opt. Lett. 36 (9) (2011) 1587–1589.
[14] R. Osellame, M. Lobino, N. Chiodo, M. Marangoni, G. Cerullo, R. Ramponi, H.T. Bookey, R.R. Thomson, N.D. Psaila, A.K. Kar, Appl. Phys. Lett. 90 (24) (2007) 241107.
[15] S. Müller, T. Calmano, P. Metz, N. Hansen, C. Kränkel, G. Huber, Opt. Lett. 37 (24) (2012) 5223–5225.
[16] S.J. Beecher, R.R. Thomson, D.T. Reid, N.D. Psaila, M. Ebrahim-Zadeh, A.K. Kar, Opt. Lett. 36 (23) (2011) 4548–4550.
[17] Y. Tan, F. Chen, J.R. Vázquez de Aldana, G.A. Torchia, A. Benayas, D. Jaque, Appl. Phys. Lett. 97 (3) (2010) 031119.
[18] W.F. Silva, C. Jacinto, A. Benayas, J.R. Vázquez de Aldana, G.A. Torchia, F. Chen, Y. Tan, D. Jaque, Opt. Lett. 35 (7) (2010) 916–918.
[19] Y. Tan, Y. Jia, F. Chen, J.R. Vázquez de Aldana, D. Jaque, J. Opt. Soc. Am. B 28 (7) (2011) 1607–1610.
[20] C. Zhang, N.N. Dong, J. Yang, F. Chen, J.R. Vázquez de Aldana, Q.M. Lu, Opt. Exp. 19 (13) (2011) 12503–12508.
[21] N. Pavel, G. Salamu, F. Voicu, F. Jipa, M. Zamfirescu, T. Dascalu, Laser Phys. Lett. 10 (9) (2013) 095802.
[22] C. Grivas, C. Corbari, G. Brambilla, P.G. Lagoudakis, Opt. Lett. 37 (22) (2012) 4630–4632.
[23] Y. Jia, F. Chen, J.R. Vázquez de Aldana, Opt. Exp. 20 (15) (2012) 16801–16806.
[24] N. Pavel, G. Salamu, F. Jipa, M. Zamfirescu, Opt. Exp. 22 (19) (2014) 23057–23065.
[25] G. Salamu, F. Jipa, M. Zamfirescu, N. Pavel, Opt. Exp. 22 (5) (2014) 5177–5182.
[26] G. Palmer, S. Gross, A. Fuerbach, D.G. Lancaster, M.J. Withford, Opt. Exp. 21 (14) (2013) 17413–17420.
[27] M.T. Hill, M.C. Gather, Nat. Photon. 8 (12) (2014) 908–918.
[28] C. Grivas, Prog. Quant. Electron. 35 (6) (2011) 159–239.
[29] J. Liu, J. Dai, S.L. Chin, X.C. Zhang, Nat. Photon. 4 (9) (2010) 627–631.
[30] D. Popa, Z. Sun, T. Hasan, F. Torrisi, F. Wang, A.C. Ferrari, Appl. Phys. Lett. 98 (7) (2011) 073106.
[31] Q. Bao, H. Zhang, Y. Wang, Z. Ni, Y. Yan, Z.X. Shen, K.P. Loh, D.Y. Tang, Adv. Funct. Mater. 19 (19) (2009) 3077–3083.
[32] J.M. Dawlaty, S. Shivaraman, J. Strait, P. George, M. Chandrashekhar, F. Rana, M.G. Spencer, D. Veksler, Y. Chen, Appl. Phys. Lett. 93 (13) (2008) 131905.
[33] Z. Sun, D. Popa, T. Hasan, F. Torrisi, F. Wang, E. Kelleher, J. Travers, V. Nicolosi, A. Ferrari, Nano Res. 3 (9) (2010) 653–660.
[34] M.E. Sánchez-Morales, G.V. Vázquez, P. Moretti, H. Márquez, Opt. Mater. 29 (7) (2007) 840–844.
[35] Y. Yao, N. Dong, F. Chen, L. Pang, Z. Wang, Q. Lu, Opt. Exp. 19 (24) (2011) 24252–24257.
[36] A. Benayas, D. Jaque, S.J. Hettrick, J.S. Wilkinson, D.P. Shepherd, J. Appl. Phys. 103 (10) (2008) 103104.
[37] H. Lia, X. Wu, R. Song, Mater. Charact. 59 (8) (2008) 1066–1069.
[38] R. He, Q. An, J.R. Vázquez de Aldana, Q. Lu, F. Chen, Appl. Opt. 52 (16) (2013) 3713–3718.